Nanoscale Advances

ROYAL SOCIETY OF CHEMISTRY

PAPER

View Article Online
View Journal | View Issue

Cite this: *Nanoscale Adv.*, 2024, **6**, 3347

Room temperature synthesis of nanocomposite thin films with embedded $Cs_2AgIn_{0.9}Bi_{0.1}Cl_6$ lead-free double perovskite nanocrystals with long-term water stability, wide range pH tolerance, and high quantum yield†

Steevanson Bayer, Jason Ho Yin Yu and Stefan Nagl *

The synthesis of $Cs_2AgIn_{0.9}Bi_{0.1}Cl_6$ nanocrystals was achieved at room temperature under ambient conditions using the ligand-assisted reprecipitation (LARP) method. The synthesized NCs exhibit bright orange emission when excited at 375 nm and have broad photoluminescence (PL) emission spectra with a maximum of 630 nm. A photoluminescence quantum yield (PLQY) of 36% was observed in these NCs without any polymer coatings. Polystyrene (PS), and poly (methyl methacrylate) (PMMA) were used to enhance the water stability and PLQY values up to 64%. Nanocomposite thin films with these polymer encapsulations exhibit good thermal stability up to at least 353 K and high quantum yields. PMMA-coated NCs showed long-term water stability for at least 4 months. The composites remain photostable when in contact with water for at least 120 min under continuous 365 nm UV illumination at 1 mW cm^{-2}. Due to their excellent optical properties, aqueous stability, and wide range pH tolerance, these nanocomposite thin films could be employed for a variety of biological applications.

Received 21st March 2024
Accepted 12th May 2024

DOI: 10.1039/d4na00233d

rsc.li/nanoscale-advances

Introduction

Lead halide perovskite nanocrystals are heavily studied due to their excellent optical properties and wide-ranging applications, but lead toxicity is still a major issue.[1,2] They have been utilized in various domains so far such as solar cells,[3–6] LEDs,[7–11] and scintillators.[12–16] Their features such as high PLQY, absorption coefficient, and easy band gap tunability,[17–21] make lead halide perovskite nanocrystals ideal candidates for different optoelectronic applications.[22–30] The stability of lead halide perovskite NCs however, is a limitation.[31,32] Factors such as elevated temperature, air, and moisture exposure lead to nanocrystal degradation and deterioration of their optoelectronic properties.[33] Due to the presence of lead ions, there is a high risk of environmental contamination,[34,35] limited biological applications,[36] and extra preventive steps are needed to inhibit lead ion leakage.[37,38]

In order to solve the lead toxicity and poor stability of lead halide perovskite NCs, a new class of lead-free double perovskite NCs is being explored.[39] The key principle of these lead-free perovskite NCs is to use two or more atoms to compensate for one Pb^{2+} ion. Various new candidates of lead-free double perovskites have been synthesized with varying shapes and sizes.

The composition can be changed with single or multiple ion doping along with employing different synthesis methods such as hydrothermal and hot-injection methods,[40] and good PLQY values could be achieved although still lower than that of lead halide perovskite NCs.[41,42] Double perovskites display the feature of STE (self-trapped excitons).[43] This phenomenon has been observed in various double perovskite nanocrystals and is considered instrumental for different optoelectronic applications.[44] STEs lead to broad emission spectra with longer PL lifetimes.

The doping of lead-free perovskites with different ions also resulted in broad emissions.[45,46] Mn-doping was explored by Manna *et al.* and increased the PLQY of $Cs_2AgInCl_6$ lead-free perovskites ten-fold.[47] Similarly, doping of Cu(II) in $Cs_2SbAgCl_6$ double perovskites has led to a drastic change in the bandgap.[48] Xia *et al.* achieved a PLQY up to 11.4% *via* trace Bi doping of $Cs_2AgIn_{0.9}Bi_{0.1}Cl_6$.[49] Due to the formation of STEs, the PL intensity depends on the ratio of dopants. This was confirmed by Hong *et al.* as serial doping of In and Bi resulted in emission changes from violet to orange emission with the increase of In concentration.[50] Different combinations of ions such as rare earth metals,[51–54] Na, and K have also been explored to synthesize more stable double perovskites with enhanced optoelectronic properties.[55]

Department of Chemistry, The Hong Kong University of Science and Technology, Kowloon, Hong Kong SAR, China. E-mail: chnagl@ust.hk

† Electronic supplementary information (ESI) available. See DOI: https://doi.org/10.1039/d4na00233d

Table 1 Composition, emission peak, and PLQY values of lead-free perovskite nanocrystals reported in the literature

Lead-free perovskite nanocrystals composition	Emission peak (nm)	PLQY (%)	References
$Cs_3Bi_2Br_9$	460	4.5	41
$Cs_2AgInCl_6$: 1% Bi	580	11	50
$Cs_2NaInCl_6$: Ag	535	31	45
$Cs_2AgIn_{0.9}Bi_{0.1}Cl_6$	650	31	64
$Cs_2AgInCl_6$: Bi/Ln	610	56	54
$Cs_2Ag_{0.17}Na_{0.83}In_{0.88}Bi_{0.12}Cl_6$	557	64	56
$Cs_2AgIn_{0.9}Bi_{0.1}Cl_6$	630	64	This work

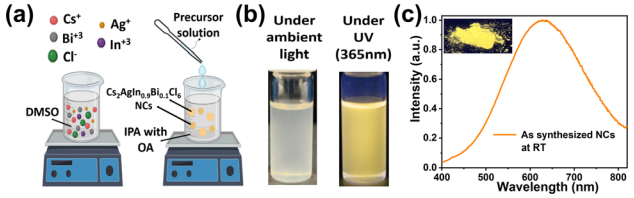

Fig. 1 (a) Schematic illustration of the synthesis of $Cs_2AgIn_{0.9}Bi_{0.1}Cl_6$ NCs. (b) Optical images of $Cs_2AgIn_{0.9}Bi_{0.1}Cl_6$ NCs dispersed in IPA under UV light (365 nm). (c) PL spectra of $Cs_2AgIn_{0.9}Bi_{0.1}Cl_6$ NCs synthesized at room temperature, 0.2 g L^{-1}, excited at 375 nm. (Inset shows powdered $Cs_2AgIn_{0.9}Bi_{0.1}Cl_6$ NCs under a UV lamp).

These results show ion doping and synthesis conditions are important factors in enhancing the optoelectronic properties of lead-free double perovskite NCs. One of the most promising lead-free perovskites is $Cs_2AgIn_{0.9}Bi_{0.1}Cl_6$ NCs as shown in Table 1. The applications of these lead-free double perovskite NCs are so far focused on LEDs[56–58] and solar cells.[59] Utilizing these NCs in an aqueous environment is still a huge challenge as it requires substantial air-, water-, and photostability of the material.[60–63]

In this study, highly stable lead-free double perovskite $Cs_2AgIn_{0.9}Bi_{0.1}Cl_6$ NCs with high PLQY values were synthesized at room temperature using the Ligand-Assisted Reprecipitation (LARP) method. We also report the successful encapsulations of lead-free double perovskite NCs into polystyrene (PS) and poly (methyl methacrylate) (PMMA) polymers.

Among these encapsulations, PMMA-coated NCs exhibit exceptional long-term water stability and wide range pH tolerance in Britton–Robinson buffer (BRB) solutions for up to 16 weeks. Polymer encapsulations provide an additional layer of protection and prevent the degradation of NCs due to external factors such as moisture, air, and heat. The composite thin films embedded with $Cs_2AgIn_{0.9}Bi_{0.1}Cl_6$ NCs exhibited strong thermal stability and can maintain close to initial PL intensities even after 5 heating–cooling cycles in the temperature range from 293 K to 353 K.

This study provides an effective strategy to enhance the optical properties of non-toxic lead-free $Cs_2AgIn_{0.9}Bi_{0.1}Cl_6$ NCs using polymer encapsulations at low temperatures while using only a single stabilizing ligand. The results could be used for biological and other applications in aqueous environments and more robust photovoltaic devices with long shelf life.

Results and discussion

The $Cs_2AgIn_{0.9}Bi_{0.1}Cl_6$ double perovskite NCs were synthesized using the ligand-assisted reprecipitation (LARP) method at room temperature as shown in Fig. 1a. Briefly, dimethyl sulfoxide (DMSO) was used to make the precursor solution as all the constituent salts readily dissolve in it with mild stirring. Oleic acid (OA) was used as the stabilizing ligand to control the size and passivation of the surface of the NCs. The precursor solution was added dropwise in isopropyl alcohol (IPA) while stirring at room temperature. The drastic change in solvent polarity leads to the formation of NCs.

The as-synthesized NCs were centrifuged and dried using a vacuum oven for 30 min at 70 °C. The as-synthesized $Cs_2AgIn_{0.9}Bi_{0.1}Cl_6$ NCs appear as a cloudy white colloidal dispersion under ambient light and exhibit bright orange emission under UV-light irradiation. The strong orange emission of $Cs_2AgIn_{0.9}Bi_{0.1}Cl_6$ NCs is a forbidden transition and possible due to STEs. The UV absorption peak is at 375 nm and the PL emission peak was observed at 630 nm (Fig. 1c and d).

Different synthesis temperatures were explored; at lower temperatures (5 °C to 15 °C), the colloidal dispersion exhibits blue emission. Moreover, even with high precursor concentration only faint orange emission was achieved at low synthesis temperatures.

For synthesis at room temperature, a bright orange emission was observed. Presumably, lower temperatures limit the proper mixing of the precursor solution and favour free exciton states leading to blue emission. The ratio of In and Bi is very critical during the synthesis as it will heavily influence the emission spectrum. The precursor concentration, synthesis temperature, and amount of oleic acid were fine tuned to get the brightest orange emission. Syntheses at higher temperatures were also tested but did not yield better results than nanocrystal preparation at room temperature.

The highest PL intensity was achieved by determining the most compatible antisolvents among IPA, toluene, hexane, and chloroform. The LARP method is highly economical as it does not require a complex setup of inert gases and high temperatures, unlike the hot injection method.

The compositional changes in perovskites can lead to a shift in emission peak and intensity. The broad peak is due to the STEs as reported and investigated earlier.[55] This was observed when the precursor was added to the antisolvent. Initially, as the solution turns cloudy, a faint blue emission is observed under the UV light but as precursor concentration increases with more drops, there is a smooth transition from blue to orange emission.

This is since correct concentration ratios have to be achieved between In and Bi (9 : 1) to reach the appropriate stoichiometric values. Similarly, in the instances where the orange emission is not stable enough, we observed that the emission returned to a blue colour. This phenomenon has been investigated by multiple researchers.[47,65]

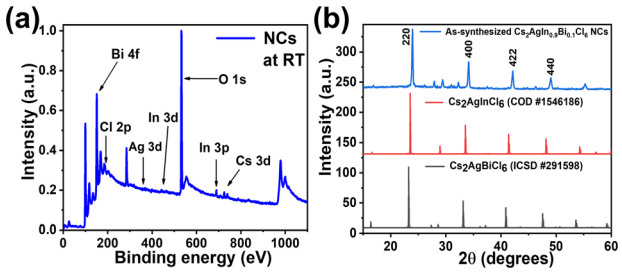

Fig. 2 (a) XPS elemental analysis of $Cs_2AgIn_{0.9}Bi_{0.1}Cl_6$ NCs synthesized at room temperature. (b) XRD pattern of $Cs_2AgIn_{0.9}Bi_{0.1}Cl_6$ NCs synthesized at room temperature with reference patterns (ICSD#244519 and COD#1546186).

X-ray photoelectron spectroscopy (XPS) measurements of the powdered samples were done to confirm the constituent elements of the double perovskite NCs. As shown in Fig. 2a, the XPS confirms he presence of all constituent elements in the double perovskite NCs. The presence of trivalent Bi^{3+} is confirmed by peaks corresponding to Bi $4f_{5/2}$ (165.7 eV) and Bi $4f_{7/2}$ (160.1 eV) in Fig. S1(b).† Similarly, a doublet peak is observed in Fig. S1(d)† due to spin–orbit coupling and assigned as In $3d_{3/2}$ (454.1 eV) and In $3d_{5/2}$ (446.3 eV).

The peak in Fig. S1(e)† corresponds to chloride ions surrounding the NCs due to their excess amount gathered from all the salts used in the precursor. X-ray diffraction (XRD) measurements of the powdered samples indicated the crystal structure of the double perovskite NCs.

The peaks of $Cs_2AgIn_{0.9}Bi_{0.1}Cl_6$ NCs exhibit similarity between the peaks of pure phases, *i.e.*, $Cs_2AgInCl_6$ and $Cs_2AgBiCl_6$ as shown in Fig. 2b for reference. The peaks are slightly shifted due to the incorporation of In and Bi into the lattice. The XRD peaks agree well with the known structure of $Cs_2AgIn_{0.9}Bi_{0.1}Cl_6$ NCs reported in the literature,[64,65] the space group of the as-synthesized NCs is $Fm\bar{3}m$ (225) as per the XRD peaks.

Additionally, the EDX elemental maps of Cs, In, Bi, Ag, and Cl showed the composition of the double perovskite NCs as shown in Fig. S2.† Transmission electron microscopy (TEM) images were taken to investigate the size of the NCs. TEM images revealed mostly spherically shaped NCs with an average diameter of 10.2 nm ± 5.6 nm (Fig. 3a). The corresponding size distribution histogram is shown in Fig. 3b. At higher magnification, mostly spherically shaped NCs with an average size of 11.6 ± 5.3 nm were observed as shown in Fig. 3c and d.

High resolution TEM (HRTEM) images were taken to observe the NCs as shown in Fig. 3e and f respectively. The appearance of the nanocrystals was found to be not uniform and different shapes and sizes of the NCs can be observed. With some size variations, the average diameter of the NCs is around 11 nm. HRTEM images were taken to observe single NCs as shown in Fig. S3(a)† and lattice fringes could be observed as shown in Fig. S3(b).† The interplanar distance between lattice fringes is in the range of 0.29 nm to 0.31 nm. Selected-area electron diffraction (SAED) patterns Fig. S3(d)† of the area shown in Fig. S3(c)† shows the Fast Fourier Transform (FFT) patterns of

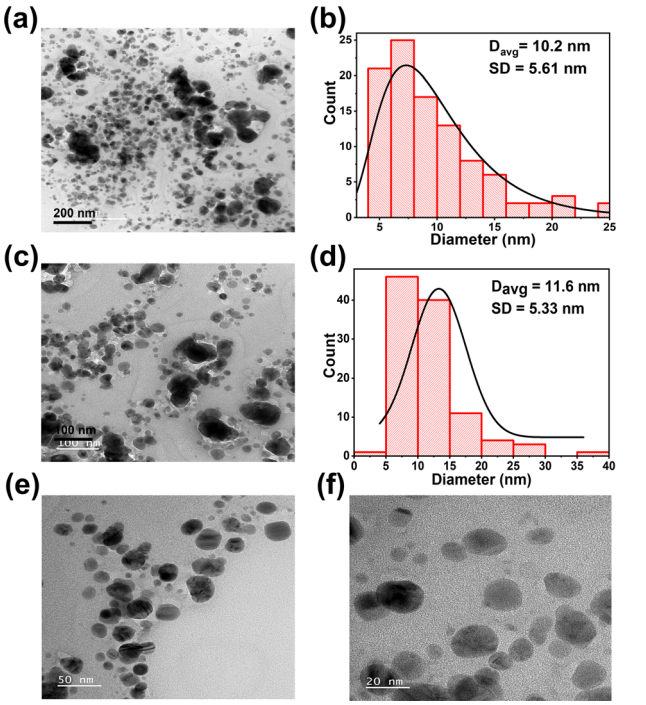

Fig. 3 (a) TEM images of $Cs_2AgIn_{0.9}Bi_{0.1}Cl_6$ NCs synthesized at room temperature. (b) Corresponding size distribution histogram. (c) High-resolution TEM (HRTEM) images of $Cs_2AgIn_{0.9}Bi_{0.1}Cl_6$ NCs. (d) corresponding size distribution histogram. Magnified images of NCs, (e) 50 nm scale bar and (f) 20 nm scale bar.

NCs. The TEM images and lattice spacing agree well with previously reported $Cs_2AgIn_{0.9}Bi_{0.1}Cl_6$ NCs in the literature.[64,65]

The synthesis temperature used plays an important role in determining the optical properties of NCs. Synthesis at room temperature resulted in a higher PLQY than other temperatures tested. OA played a significant role in the synthesis of NCs as without the ligand the emission is faint and unstable.

The addition of OA allows better control of the size of the NCs and leads to a higher shelf life. In the case of lead perovskite nanocrystals, metal–organic frameworks (MOFs)[66–69] and different polymer encapsulations have been heavily exploited to tune and enhance the NCs optoelectronic and thermal properties as well as water stability.[70–74]

Here PS and PMMA were utilized to enhance the optical properties of the as-synthesized $Cs_2AgIn_{0.9}Bi_{0.1}Cl_6$ NCs. Similarly, in this study, the PLQY was observed in the range of 36% to 64% depending on the synthesis conditions and polymers used as summarized in Table 2.

Moreover, no large micro-particles are observed. Hence, room temperature synthesis leads to a good quality of the NCs, which compares favourably with reported literature where a higher temperature and a complex gas setup were required to synthesize NCs with bright PL emission.[45,55,57,64]

Different polymers such as polyvinylidene fluoride (PVDF) and poly-2-hydroxyethylmethacrylate (pHEMA) were also tested but the PL enhancement and stability was lower and a larger average particle size was observed, presumably due to aggregation.

Table 2 Dependence of PLQY of nanoparticles on polymer encapsulations, measured at a conc. of 0.2 g L^{-1} in isopropanol, respectively

Polymer used	Synthesized at room temperature (PLQY)
None	36%
PS	64%
PMMA	61%

The PL emission of PS-coated NCs was found to be slightly higher than PMMA-coated ones although both materials showed good results (Fig. 4). Different polymer coatings are known to be compatible with lead-free perovskite NCs as shown by Xu *et al.*[75,76] Similar PLQY enhancements were observed in the case of PMMA and PS encapsulations of methylammonium lead bromide perovskite nanocrystals. A solvent-free ball milling method was used for the encapsulation in those works.[77]

Photoluminescence lifetimes (PL) were recorded using time-correlated single photon counting. Without any polymer coating, the average PL lifetime was observed as 694 ns as shown in Fig. 5a. The lifetime values longer than 100 ns suggest the presence of STEs in the lead-free double perovskite NCs. For PS-coated NCs, the PL was increased to 760 ns, and for PMMA-coated NCs, the PL was increased to 797 ns as displayed in Fig. 5b and c respectively. The average lifetime, radiative, and non-radiative lifetimes are summarized in Table S2.†

Composite thin films of $Cs_2AgIn_{0.9}Bi_{0.1}Cl_6$ NCs with polymers were fabricated using the drop-casting method. The polymer-coated NCs colloidal dispersion was drop-casted on an ITO glass substrate and annealed on a hot plate at 100 °C for 30 min.

A temperature calibration setup fabricated in-house was used to change the temperature of the thin film between 20 °C and 80 °C. The temperature was allowed to stabilize for 10 min before each measurement. A pronounced dependency of PL intensity to temperature was found for all materials, with a sharp drop at 80 °C, while the emission recovered to varying extents when the temperature was lowered to 20 °C.

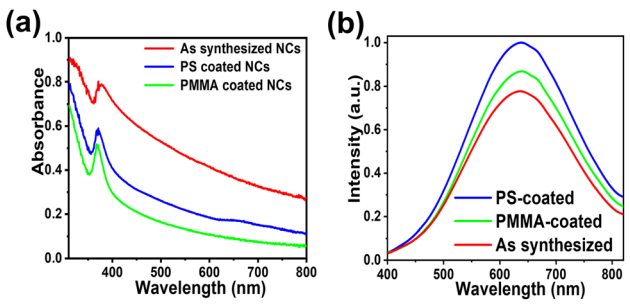

Fig. 4 (a) UV-Vis absorption spectra of different polymer-coated NCs (0.2 g L^{-1} in isopropanol) colloidal mixtures synthesized at RT. (b) PL emission spectra (excited at 375 nm) of different NCs colloidal mixture synthesized at RT.

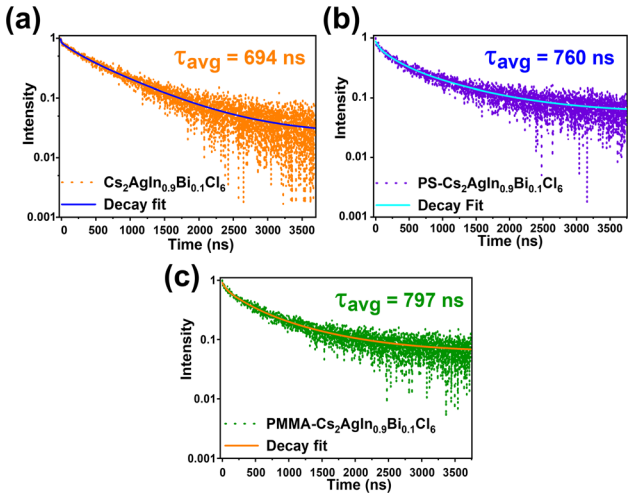

Fig. 5 TRPL of different samples in (0.2 g L^{-1} in isopropanol, 360 nm fs laser excitation), (a) as-synthesized $Cs_2AgIn_{0.9}Bi_{0.1}Cl_6$ NCs, (b) PS-coated $Cs_2AgIn_{0.9}Bi_{0.1}Cl_6$ NCs and (c) PMMA-coated $Cs_2AgIn_{0.9}Bi_{0.1}Cl_6$ NCs lifetime measurements with decay fit.

PS and PMMA-coated NCs composite thin films exhibited superior thermal stability compared to thin films of NCs without polymer encapsulation. For NCs without polymer coating, at high temperatures, the PL intensity was observed to drop drastically with little reversibility. Among the two composite thin films, the PMMA-coated NCs thin film showed the highest thermal stability and best reversibility as compared to the PS-coated NCs thin film (Fig. S4a and b†).

Photostability tests were also carried out to see the stability of PS and PMMA-coated $Cs_2AgIn_{0.9}Bi_{0.1}Cl_6$ NCs composite thin film under continuous 365 nm UV illumination at 1 mW cm^{-2} for 120 min with constant contact with a 100 μL DI droplet on the composite thin film as shown in Fig. S4c.† As displayed in Fig. S4d,† the PMMA-coated $Cs_2AgIn_{0.9}Bi_{0.1}Cl_6$ thin film showed good photostability when in contact with a 100 μL droplet of BRB buffer solutions of different pH values. This provides evidence that the composite films are photostable in different environments and their optoelectronic properties are not diminished drastically.

PS and PMMA-coated $Cs_2AgIn_{0.9}Bi_{0.1}Cl_6$ NCs composite thin films were tested for water and pH stability. As shown in Fig. S5(a),† initially, without any polymer coating, the contact angle of $Cs_2AgIn_{0.9}Bi_{0.1}Cl_6$ NCs composite thin film was observed to be 48°. Contact angle measurements were performed using water droplets and confirmed the increase in hydrophobicity when PS and PMMA coatings were applied as shown in Fig. S5(b) and (c).† The roughness of thin films is compared in Fig. S6(a) and (b),† indicating that PMMA-coated thin films have a smoother surface morphology.

In the case of PMMA-coated and PS-coated $Cs_2AgIn_{0.9}Bi_{0.1}Cl_6$ NCs composite thin films, the angle was 87° and 90°, respectively.

Due to the polymer protection, the encapsulated NCs exhibited good water stability and strong pH tolerance for at least 16 weeks, which exceeds the reported literature so far as

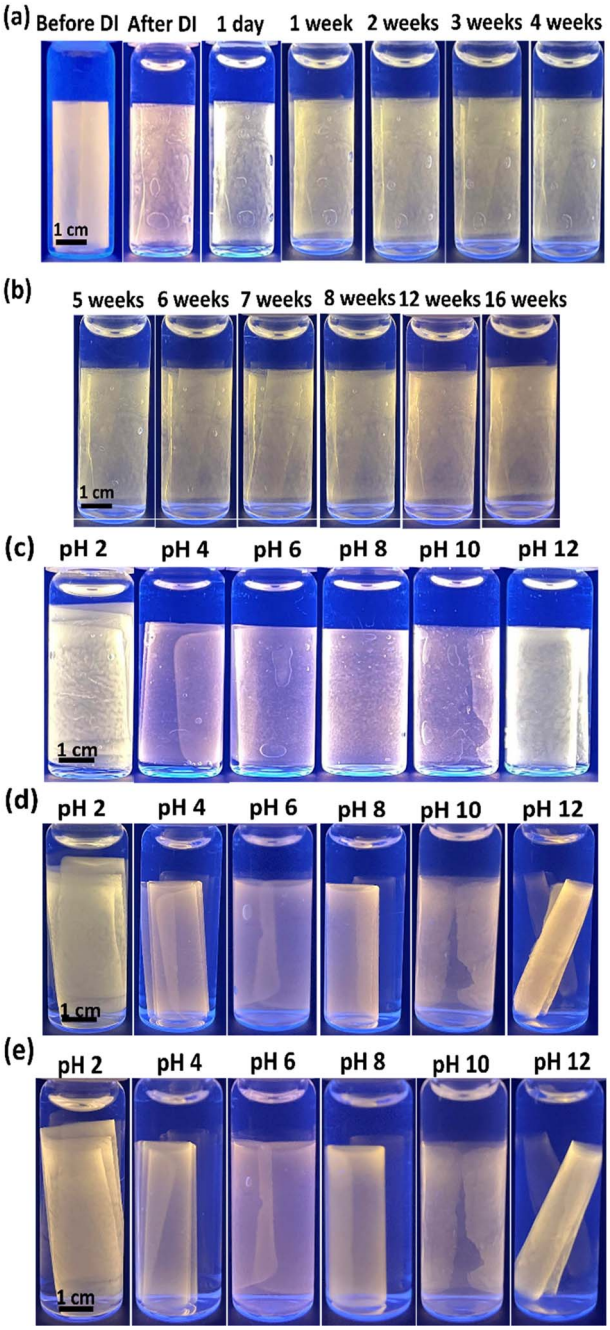

Fig. 6 (a) Photographs of PMMA-coated $Cs_2AgIn_{0.9}Bi_{0.1}Cl_6$ thin films immersed in 4 mL DI water over a period of up to 16 weeks taken under UV (365 nm). (b) Initial photographs of PMMA-coated $Cs_2AgIn_{0.9}Bi_{0.1}Cl_6$ thin films immersed in 4 mL BRB solution of different pH water under UV lamp excitation ranging from pH 2–12. (c) Photographs of the thin films in (b) after 8 weeks and (d) after 16 weeks immersion into buffer solutions.

summarized in Table S1.† As shown in Fig. 6(a)–(d) the orange emission stays constant even after 16 weeks. Also, when exposed to the BRB buffer ranging from pH 2 to pH 12, emission of various intensities is observed even after 16 weeks. At higher pH values, the composite thin film tends to get wrapped towards the inside.

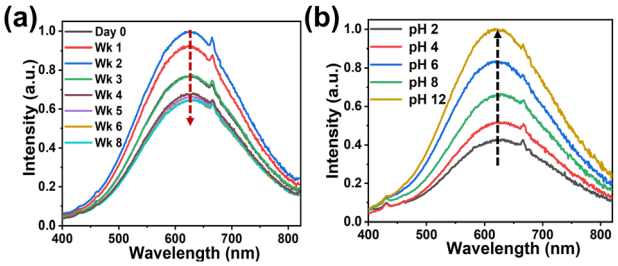

Fig. 7 (a) PL spectra of PMMA-coated $Cs_2AgIn_{0.9}Bi_{0.1}Cl_6$ thin films immersed in DI water monitored for two months, excited at 375 nm. (b) PL spectra of PMMA-coated $Cs_2AgIn_{0.9}Bi_{0.1}Cl_6$ thin films immersed in BRB solution of different pH values.

The PL intensities of these submerged composite thin films are pH-dependent and the composite films were fully immersed in DI and BRB buffers of different pH values from 2 to 12. Even at extreme pH conditions, the PMMA-coated NCs exhibited high stability and bright emission.

Weekly images were taken for these submerged samples over a time period of 16 weeks as shown in Fig. S7.† The presence of ions such as Na^+ and K^+ in the environment of the NCs has been shown to enhance the PL emission intensity by passivating the surface of the NCs.[78,79] At pH 12, the Na^+ ion concentration in the BRB buffer would be highest and it enhances the emission intensity as seen in Fig. 7.

As shown in Fig. 7a, there is a gradual increase in PL emission in the first week, followed by a gradual decrease in the subsequent week when exposed to DI. The PL emission decreases by 12% over the period of two months. Fig. 7b shows the increase in PL intensities with change in pH. The PL emission increases from pH 2 to 12 by around 132%.

Some shoulder peaks are observed in the PL measurements as shown in Fig. 7a and b at 667 nm. Presumably these are scattering peaks caused by some degree of aggregation during the process of thin film formation.

The strong water and pH stability make these polymer-coated lead-free double perovskite NCs a potential candidate in replacing the toxic lead-based crystals[80–84] and contributing to a more sustainable ecosystem.[85,86]

Water stable lead-free NCs embedded thin films provide a better alternative to the conventional lead perovskite nanocrystals for various biomedical and optoelectronic applications. Combined with their non-toxic nature, PS and PMMA-coated $Cs_2AgIn_{0.9}Bi_{0.1}Cl_6$ NCs composite thin film could be used as fluorescence labels or probes in biological mediums to monitor various reactions and processes in various pH environments and with long-term water exposure.

Conclusions

In summary, we have successfully synthesized lead-free double perovskite nanocrystals at room temperature using the simple, cost-effective LARP method without using a high temperature and inert gases setup. The perovskite NCs were successfully encapsulated into different polymers such as PS and PMMA.

The optical properties such as PLQY and stability in the ambient environment were enhanced with the polymer encapsulations. The use of polymers is a more feasible way to tune the PL properties without using expensive rare earth metals as dopants. Potentially, the encapsulation with the polymers and methods used herein could also be performed with different nanocrystals or different nanocrystal synthesis procedures.

The composite thin films exhibited good temperature and aqueous stability. PMMA-coated NC composite films exhibit exceptional long-term water stability and pH resistance even after 16 weeks. This feature may be used for making wide range pH resistant sensing layers for biomedical applications. This study opens up exciting opportunities for lead-free double perovskite NCs in the field of composite-based biological applications and solve the existing stability issues in aqueous systems and harsh pH conditions.

Experimental section

Materials

All chemicals were of analytical grade unless specified otherwise. CsCl, AgCl, $InCl_3$, $BiCl_3$, and oleic acid (OA, 99%) were supplied from Sigma-Aldrich, USA. DMSO was obtained from J&K-Chemical Co., HK. Isopropyl alcohol (IPA), toluene, and hexane were obtained from Acros Organics. Polystyrene MW 35 000 (PS), poly (methyl methacrylate) MW 25 000 (PMMA), and poly (vinylidene fluoride) (PVDF) MW 180 000 (PVDF) were purchased from Sigma-Aldrich, USA.

Synthesis of lead-free double perovskite ($Cs_2AgIn_{0.9}Bi_{0.1}Cl_6$) NCs

CsCl (500 μmol), AgCl (250 μmol), $InCl_3$ (225 μmol), and $BiCl_3$ (25 μmol) were dissolved in 10 mL DMSO by vigorously stirring on a magnetic stirrer for 10 min. After getting the clear solution 2 mL of OA (oleic acid) was added to the precursor solution. 300 μL of this precursor solution was added dropwise in 5 mL isopropanol solution while stirring the solution vigorously. The solution turns cloudy as more precursor is added. The emission color is blue initially but with more drops, it turns to bright orange. The dried powder was redispersed in various antisolvents such as IPA, toluene, and hexane for further use.

Fabrication of $Cs_2AgIn_{0.9}Bi_{0.1}Cl_6$ NCs embedded composite thin films

PS (5% w/w) and PMMA (5% w/w) solutions were made by dissolving the polymer in 5 mL of toluene and stirring overnight for complete mixing. 2.5 mL of $Cs_2AgIn_{0.9}Bi_{0.1}Cl_6$ NCs in toluene (2 g L^{-1}) was added to the clear polymer solution while stirring for 10 min. 2 mL of this solution was dropcast on an ITO glass and annealed at 100 °C for 30 min. A thin film with bright orange emission was formed after complete solvent evaporation. Dried thin films were used for further studies.

Characterization

Photoluminescence (PL) spectra and photoluminescence quantum yield (PLQY) measurements were performed on a fluorescence spectrometer (FS5 Spectrofluorometer, Edinburgh, UK). UV-Vis absorption spectra were measured using a UV-Vis spectrometer (Cary 60, Varian, United States).

All the optical measurements (UV, PL, PLQY) described above were carried by dispersing NCs at 0.2 g L^{-1} in IPA. For absolute PLQY measurements, the absolute error is ± 3%. TEM images were acquired on a JEM-2010, JEOL, Japan transmission electron microscope and High-resolution TEM images were acquired using a JEM-ARM200F (JEOL).

X-ray photoelectron spectroscopy (XPS) was performed using an X-ray photoelectron spectrometer equipped with an Al Kα X-ray source. All XPS samples were prepared by drop-casting of NCs dispersed in IPA and dried on silicon substrates (0.6 × 0.6 cm^2).

An inverted microscope (Eclipse Ti2, Nikon, Japan) with a CCD camera (Imagex-nano CCD, Photonic Research Systems, UK) was used to characterize various composite films and measure PL intensities. For the observation of fluorescence images of the films, a 4X (NA 0.20, Plan Apo, Nikon, Japan) was used. Thermal and photostability studies were performed with the same objective. A near UV LED (3M365L2, Thorlabs, USA) light source was used for excitation. The contact angle of different polymer-coated $Cs_2AgIn_{0.9}Bi_{0.1}Cl_6$ NC thin films was measured by a contact angle meter (Theta lite, Biolin Scientific, Sweden). The roughness and thickness were measured by an optical profiler (3D Optical Profilometer NPFLEX-1000, Bruker).

Time-resolved photoluminescence (TRPL) was carried out by exciting the sample with a 360 nm, 100 fs laser generated by frequency doubling the output of a mode locked titanium sapphire oscillator laser tuned to 720 nm. The output light from the laser was pulse-picked down to 250 kHz pulse rate, and the maximal pulse intensity was equal to 200 nJ cm^{-2}. The emission was led into an Acton Spectrapro 275 monochromator (USA) by a pair of achromatic lenses and passed through a 435 nm long-pass filter and was collected by a time-correlated single photon counting (TCSPC) system (Becker and Hickl, Germany).

Author contributions

S. B. and S. N. conceived the project, designed experiments, and wrote the manuscript. S. B. and J. H. Y. Y. performed experiments. S. N. acquired funding.

Conflicts of interest

There are no conflicts to declare.

Acknowledgements

This work was partially supported by the Hong Kong Research Grants Council (RGC, project 16309423) and the University Grants Committee (UGC, R9375). We acknowledge the services of the Materials Characterization and Preparation Facility (MCPF) at the Hong Kong University of Science and Technology (HKUST) for the characterization of lead-free double perovskite

NCs. We are grateful to Dr A. Sergeev and Prof. K. S. Wong (Dept. of Physics, HKUST) for their assistance with photoluminescence lifetime measurements.

References

1 S. Javad, A. Urban, M. Imran, L. Trizio and L. Manna, *Chem. Rev.*, 2019, 3296–3348.
2 D. Amrita, J. Ye, A. De, E. Debroye, S. Kyun Ha, E. Bladt and A. S. Kshirsagar, *ACS Nano*, 2021, **15**, 10775–10981.
3 M. A. Green, A. H. Baillie and H. J. Snaith, *Nat. Photonics*, 2014, **8**, 506–514.
4 N. J. Jeon, J. H. Noh, Y. C. Kim, W. S. Yang, S. Ryu and S. I. Seok, *Nat. Mater.*, 2014, **13**, 897–903.
5 K. T. Cho, S. Paek, G. Grancini, C. R. Carmona, P. Gao, Y. Lee and M. K. Nazeeruddin, *Energy Environ. Sci.*, 2017, **10**, 621–627.
6 S. D. Stranks and H. J. Snaith, *Nat. Nanotechnol.*, 2015, 391–402.
7 Q. A. Akkerman, M. Gandini, F. D. Stasio, P. Rastogi, F. Palazon, G. Bertoni, J. M. Ball, M. Prato, A. Petrozza and L. Manna, *Nat. Energy*, 2016, 1–7.
8 Y. Hassan, J. H. Park, M. L. Crawford, A. Sadhanala, J. Lee, J. C. Sadighian, E. Mosconi, B. R. Lee and H. J. Snaith, *Nature*, 2021, **591**, 72–77.
9 M. H. Park, J. Park, J. Lee, H. S. So, H. Kim, S. H. Jeong, T. H. Han, C. Wolf, H. Lee, S. Y and T. W. Lee, *Adv. Funct. Mater.*, 2019, **29**, 1902017.
10 Y. Shen, L. P. Cheng, Y. Q. Li, W. Li, J. D. Chen, S. T. Lee and J. X. Tang, *Adv. Mater.*, 2019, **31**, 1901517.
11 K. Lin, J. Xing, L. N. Quan, F. P. G. Arquer, X. Gong, J. Lu, L. Xie, W. Zhao, C. Yan, W. Li, X. Liu, Y. Lu, J. Kirman, E. H. Sargent, Q. Xiong and Z. Wei, *Nature*, 2018, **562**, 245–248.
12 G. Marina, I. Villa, M. Beretta, C. Gotti, M. Imran, F. Carulli and E. Fantuzzi, *Nat. Nanotechnol.*, 2020, **15**, 462–468.
13 M. Li, Y. Wang, L. Yang, Z. Chai, Y. Wang and S. Wang, *Angew. Chem., Int. Ed.*, 2022, **134**, e202208440.
14 F. Zhou, Z. Li, W. Lan, Q. Wang, L. Ding and Z. Jin, *Small Methods*, 2020, **4**, 2000506.
15 A. Jana, S. Cho, S. A. Patil, A. Meena, Y. Jo, V. G. Sree, Y. Park, H. Kim, H. Im and R. A. Taylor, *Mater. Today*, 2022, **55**, 110–136.
16 M. D. Birowosuto, D. Cortecchia, W. Drozdowski, K. Brylew, W. Lachmanski, A. Bruno and C. Soci, *Sci. Rep.*, 2016, **6**, 37254.
17 L. Protesescu, S. Yakunin, M. I. Bodnarchuk, F. Krieg, R. Caputo, C. H. Hendon, R. X. Yang, A. Walsh and M. V. Kovalenko, *Nano Lett.*, 2015, **15**, 3692–3696.
18 S. Liu, G. Chen, Y. Huang, S. Lin, Y. Zhang, M. He, W. Xiang and X. Liang, *J. Alloys Compd.*, 2017, **724**, 889–896.
19 D. N. Minh, J. Kim, J. Hyon, J. H. Sim, H. H. Sowlih, C. Seo, J. Nam, S. Eom, S. Suk, S. Lee, E. Kim and Y. Kang, *Chem. Mater.*, 2017, **29**, 5713–5719.
20 H. Huang, L. Polavarapu, J. A. Sichert, A. S. Susha, A. S. Urban and A. L. Rogach, *NPG Asia Mater.*, 2016, **8**, e328.
21 L. Wu, Q. Zhong, D. Yang, M. Chen, H. Hu, Q. Pan, H. Liu, M. Cao, Y. Xu, B. Sun and Q. Zhang, *Langmuir*, 2017, **33**, 12689–12696.
22 A. Sharenko and M. F. Toney, *J. Am. Chem. Soc.*, 2016, **138**, 463–470.
23 Y. Wang, X. Li, V. Nalla, H. Zeng and H. Sun, *Adv. Funct. Mater.*, 2017, **27**, 1605088.
24 F. Yan, J. Xing, G. Xing, L. Quan, S. T. Tan, J. Zhao, R. Su, L. Zhang, S. Chen, Y. Zhao, A. Huan, E. H. Sargent, Q. Xiong and H. V. Demir, *Nano Lett.*, 2018, **18**, 3157–3164.
25 Q. Lai, L. Zhu, Y. Pang, L. Xu, J. Chen, Z. Ren, J. Luo, L. Wang, L. Chen, K. Han, P. Lin, D. Li, S. Lin, B. Chen, C. Pan and Z. L. Wang, *ACS Nano*, 2018, **12**, 10501–10508.
26 Y. Zhan, Y. Wang, Q. Cheng, C. Li, K. Li, H. Li, J. Peng, B. Lu, Y. Wang, Y. Song, L. Jiang and M. Li, *Angew. Chem., Int. Ed.*, 2019, **58**, 16456–16462.
27 Z. Lu, Y. Li, W. Qiu, A. L. Rogach and S. Nagl, *ACS Appl. Mater. Interfaces*, 2020, **12**, 19805–19812.
28 S. Li, D. Lei, W. Ren, X. Guo, S. Wu, Y. Zhu, A. L. Rogach, M. Chhowalla and A. K. Y. Jen, *Nat. Commun.*, 2020, **11**, 1192.
29 H. J. Kim, H. Oh, T. Kim, D. Kim and M. Park, *ACS Appl. Nano Mater.*, 2022, **5**, 1308–1316.
30 Z. Lu, Y. Li, Y. Xue, W. Zhou, S. Bayer, I. D. Williams, A. L. Rogach and S. Nagl, *ACS Appl. Nano Mater.*, 2022, **5**, 5025–5034.
31 G. H. Ahmed, J. Yin, O. M. Bakr and O. F. Mohammed, *ACS Energy Lett.*, 2021, 1340–1357.
32 H. Huang, M. I. Bodnarchuk, S. V. Kershaw, M. V. Kovalenko and A. L. Rogach, *ACS Energy Lett.*, 2017, **2**, 2071–2083.
33 B. Chen, S. Wang, Y. Song, C. Li and F. Hao, *Chem. Eng.*, 2022, **430**, 132701.
34 M. Ren, X. Qian, Y. Chen, T. Wang and Y. Zhao, *J. Hazard. Mater.*, 2022, **426**, 127848.
35 G. Schileo and G. Grancini, *J. Mater. Chem. C*, 2021, **9**, 67–76.
36 G. Getachew, A. Wibrianto, A. S. Rasal, W. B. Direrssa and J. Y. Chang, *Coord. Chem. Rev.*, 2023, **482**, 215073.
37 L. Gomez, C. Weerd, J. L. Hueso and T. Gregorkiewicz, *Nanoscale*, 2017, **9**, 631–636.
38 K. Ma, X. Li, F. Yang and H. Liu, *Coatings*, 2023, **13**, 1009.
39 H. Tang, Y. Xu, X. Hu, Q. Hu, T. Chen, W. Jiang, L. Wang and W. Jiang, *Adv. Sci.*, 2021, **8**, 2004118.
40 S. Ghosh, H. Shankar and P. Kar, *Mater. Adv.*, 2022, **3**, 3742–3765.
41 B. Yang, J. Chen, F. Hong, X. Mao, K. Zheng, S. Yang, Y. Li, T. Pullerits, W. Deng and K. Han, *Angew. Chem., Int. Ed.*, 2017, **56**, 12471–12475.
42 J. Zhang, Y. Yang, H. Deng, U. Farooq, X. Yang, J. Khan, J. Tang and H. Song, *ACS Nano*, 2017, **11**, 9294–9302.
43 M. Cong, Q. Zhang, B. Yang, J. Chen, J. Xiao, D. Zheng, T. Zheng, C. Zhang and K. Han, *Nano Lett.*, 2021, **21**, 8671–8678.
44 P. Han, X. Zhang, C. Luo, W. Zhou, S. Yang, J. Zhao, W. Deng and K. Han, *ACS Cent. Sci.*, 2020, **6**, 566–572.
45 P. Han, X. Mao, S. Yang, F. Zhang, B. Yang, D. Wei, W. Deng and K. Han, *Angew. Chem., Int. Ed.*, 2019, **131**, 17391–17395.
46 Y. Jing, Y. Liu, J. Zhao and Z. Xia, *J. Phys. Chem. Lett.*, 2019, **10**, 7439–7444.

47 F. Locardi, M. Cirignano, D. Baranov, Z. Dang, M. Prato, F. Drago, M. Ferretti, L. D. Trizio and L. Manna, *J. Am. Chem. Soc.*, 2018, **140**, 12989–12995.
48 A. Karmakar, M. S. Dodd, S. Agnihotri, E. Ravera and V. K. Michaelis, *Chem. Mater.*, 2018, **30**, 8280–8290.
49 Y. Liu, Y. Jing, J. Zhao, Q. Liu and Z. Xia, *Chem. Mater.*, 2019, **31**, 3333–3339.
50 B. Yang, X. Mao, F. Hong, W. Meng, Y. Tang, X. Xia, S. Yang, W. Deng and K. Han, *J. Am. Chem. Soc.*, 2018, **140**, 17001–17006.
51 H. Yin, Q. Kong, R. Zhang, D. Zheng, B. Yang and K. Han, *Sci. China Mater.*, 2021, **64**, 2667–2674.
52 J. Liao, P. Zhang, X. Niu, H. Hong, H. Yin, Z. Li, Y. Hang and Z. Chen, *J. Alloys Compd.*, 2022, **911**, 164946.
53 N. Chen, T. Cai, W. Li, K. H. Kimball, H. Yang, M. Que, Y. Nagaoka, R. Zia and O. Chen, *ACS Appl. Mater. Interfaces*, 2019, **11**, 16855–16863.
54 S. Jin, R. Li, H. Huang, N. Jiang, J. Lin, S. Wang, Y. Zheng, X. Chen and D. Chen, *Light: Sci. Appl.*, 2022, **11**, 52.
55 Z. Liu, J. Zito, M. Ghini, L. Goldoni, M. Prato, H. B. Jalali, I. Infante, L. D. Trizio and L. Manna, *Nano Lett.*, 2022, **22**, 8567–8573.
56 Q. Hu, G. Niu, Z. Zheng, S. Li, Y. Zhang, H. Song, T. Zhai and J. Tang, *Small*, 2019, **15**, 1903496.
57 J. Luo, X. Wang, S. Li, J. Liu, Y. Guo, G. Niu, L. Yao, Y. Yan, E. H. Sargent and J. Tang, *Nature*, 2018, **563**, 541–545.
58 Q. Guo, X. Zhao, B. Song, J. Luo and J. Tang, *Adv. Mater.*, 2022, 2201008.
59 R. Ahmad, G. V. Nutan, D. Singh, G. Gupta, U. Soni, S. Sapra and R. Srivastava, *Nano Res.*, 2021, **14**, 1126–1134.
60 B. Lyu, X. Guo, D. Gao, M. Kou, Y. Yu, J. Ma, S. Chen, H. Wang, Y. Zhang and X. Bao, *J. Hazard. Mater.*, 2021, **403**, 123967.
61 A. Wang, Y. Guo, F. Muhammad and Z. Deng, *Chem. Mater.*, 2017, **29**, 6493–6501.
62 Y. Lee, J. H. Cha, H. Kim, J. Y. Lee, M. W. Lee, H. S. Jang and D. Y. Jung, *ACS Appl. Nano Mater.*, 2022, **5**, 18409–18416.
63 J. L. Xie, Z. Q. Huang, B. Wang, W. J. Chen, W. X. Lu, X. Liu and J. L. Song, *Nanoscale*, 2019, **11**, 6719–6726.
64 Y. Zhang, Z. Zhang, W. Yu, Y. He, Z. Chen, L. Xiao, J. Shi, X. Guo, S. Wang and B. Qu, *Adv. Sci.*, 2022, 2102895.
65 A. Mushtaq, B. Pradhan, D. Kushavah, Y. Zhang, M. Wolf, N. Schrenker, E. Fron, S. Bals, J. Hofkens, E. Debroye and S. K. Pal, *ACS Photonics*, 2021, **8**, 3365–3374.
66 H. Tsai, S. Shrestha, R. A. Vilá, W. Huang, C. Liu, C. H. Hou, H. H. Huang, X. Ma and W. Nie, *Nat. Photonics*, 2021, **15**, 843–849.
67 W. Nie and H. Tsai, *J. Mater. Chem. A*, 2022, **10**, 19518–19533.
68 J. Hou, Z. Wang, P. Chen, V. Chen, A. K. Cheetham and L. Wang, *Angew. Chem., Int. Ed.*, 2020, **132**, 19602–19617.
69 S. Liang, M. Zhang, G. M. Biesold, W. Choi, Y. He, Z. Li, D. Shen and Z. Lin, *Adv. Mater.*, 2021, **33**, 2005888.
70 S. K. Avugadda, A. Castelli, B. Dhanabalan, T. Fernandez, N. Silvestri, C. Collantes, D. Baranov, M. Imran, L. Manna, T. Pellegrino and M. P. Arciniegas, *ACS Nano*, 2022, **16**, 13657–13666.
71 M. R. Kar, S. Kumar, T. K. Acharya, C. Goswami and S. Bhaumik, *RSC Adv.*, 2023, **13**, 5946–5956.
72 S. Bera and N. Pradhan, *ACS Energy Lett.*, 2020, **5**, 2858–2872.
73 C. Zhang, J. Chen, L. Kong, L. Wang, S. Wang, W. Chen, R. Mao, L. Turyanska, G. Jia and X. Yang, *Adv. Funct. Mater.*, 2021, **31**, 2100438.
74 Y. Wang, L. Varadi, A. Trinchi, J. Shen, Y. Zhu, G. Wei and C. Li, *Small*, 2018, **14**, 1803156.
75 J. Shi, M. Wang, C. Zhang, J. Wang, Y. Zhou, Y. Xu and N. V. Gaponenko, *J. Mater. Chem. C*, 2023, **11**, 4742–4752.
76 A. Sahoo, T. Paul, A. Nath, S. Maiti, P. Kumar, P. Ghosh and R. Banerjee, *Nanoscale*, 2023, **15**, 11603–11615.
77 B. A. Huisman and H. J. Bolink, *Adv. Opt. Mater.*, 2023, 2202921.
78 W. Song, Y. Xie, W. Jiang, B. Liu, K. Shi and K. Pan, *Chin. Chem. Lett.*, 2023, 108521.
79 S. Li, Z. Shi, F. Zhang, L. Wang, Z. Ma, D. Wu, D. Yang, X. Chen, Y. Tian, Y. Zhang, C. Shan and X. Li, *ACS Appl. Mater. Interfaces*, 2020, **12**, 46330–46339.
80 C. H. Chen, S. N. Cheng, L. Cheng, Z. K. Wang and L. S. Liao, *Adv. Energy Mater.*, 2023, **13**, 2204144.
81 P. Billen, E. Leccisi, S. Dastidar, S. Li, L. Lobaton, S. Spatari, A. T. Fafarman, V. M. Fthenakis and J. B. Baxter, *Energy*, 2019, **166**, 1089–1096.
82 J. Liang, X. Hu, C. Wang, C. Liang, C. Chen, M. Xiao, J. Li, C. Tao, G. Xing, R. Yu, W. Ke and G. Fang, *Joule*, 2022, **6**, 816–833.
83 A. Babayigit, D. D. Thanh, A. Ethirajan, J. Manca, M. Muller, H. G. Boyen and B. Conings, *Sci. Rep.*, 2016, **6**, 18721.
84 C. Ponti, G. Nasti, D. Di. Girolamo, I. Cantone, F. A. Alharthi and A. Abate, *Trends Ecol. Evol.*, 2022, **37**, 281–283.
85 M. Lyu, J. H. Yun, P. Chen, M. Hao and L. Wang, *Adv. Energy Mater.*, 2017, **7**, 1602512.
86 X. Li, J. Shi, J. Chen, Z. Tan and H. Lei, *Materials*, 2023, **16**, 4490.